Electric Power Systems Research 235 (2024) 110866

Contents lists available at ScienceDirect

Electric Power Systems Research

journal homepage: www.elsevier.com/locate/epsr

Effects of macromodeling on the simulation of transient events caused by direct lightning to overhead power lines

Erika Stracqualursi [a,*], Rodolfo Araneo [a], Amedeo Andreotti [b], José Brandão Faria [c], Fernando H. Silveira [d], Silverio Visacro [d]

[a] Electrical Engineering Division of DIAEE, University of Rome, "Sapienza", Rome, 00184, Italy
[b] Department of Information Technology and Electrical Engineering, University of Naples Federico II, Napoli, 80125, Italy
[c] Instituto de Telecomunicacoes, Instituto Superior Tecnico – Universidade de Lisboa, Lisboa, 1049-001, Portugal
[d] Universidade Federal de Minas Gerais, Belo Horizonte, 31270-901, Brazil

ARTICLE INFO

Keywords:
Direct lightning strikes to transmission lines
Electromagnetic coupling
Electromagnetic transients
Tower model
Transmission line modeling

ABSTRACT

This paper aims at assessing the relevance of the coupling effects among the main components of overhead power lines in their lightning response, namely, tower, grounding electrodes, and shield wire(s). Mutual coupling effects are investigated by simulation, using an electromagnetic model. The analyses are performed in the frequency and time domain, by considering, respectively, the input impedance at the node of current injection and the overvoltages rising at the same node. The study is conducted considering different configurations for current excitation and three arrangements of grounding electrodes, with the corresponding soil properties. From the analysis of the results, it appears that the effects of electromagnetic coupling among the considered system components affects only marginally the lightning response of the line, being much less relevant than the effects of the uncertainties on the values of electrical parameters of the local soil. This confirms the validity of the macromodeling approach and denotes that the accuracy of the results is overall dependent on the suitability of models adopted for each component; in particular, the proper representation of the grounding system is proven as essential to the successful prediction of overvoltages at the tower top.

1. Introduction

The assessment of the lightning performance of overhead power lines is a complex matter due to the variety of existing transmission line configurations comprising different arrangements and type of components (e.g., shield wires, additional ground wires, metal oxide varistors, surge arresters, insulators, towers, and tower grounding grids). Resorting to the fundamental equations of electromagnetism for their simulation would result in significant complexity and an enormous computational burden. The macromodeling approach is a well-established methodology for solving such complex systems, and several commercial simulators of electromagnetic (EM) transients are based on this solver paradigm. The procedure characterizes single devices as independent elements of more structured systems [1]. The macromodels of each subsystem are successively interconnected through their ports to simulate the behavior of the whole system under analysis.

In this framework, the present work aims at investigating the relevance of the effect of the EM coupling among line components, usually neglected by the macromodeling approach, on the results of lightning performance studies. Indeed, while mutual EM coupling is considered for the line conductors through the application of the telegraphers equations for multiconductor transmission lines supporting quasi-TEM propagation [2], independent macro-models are adopted for transmission towers and grounding electrodes connected to their foundations. Even when EM approaches are used [3], the coupling effects between tower and grounding systems are usually not investigated, although being of potential concern.

Various techniques have been proposed in the literature for tower modeling [4,5] and simulation as a component of complex power systems [6,7]. These can be classified into lossless uniform transmission lines (TLs), non-uniform TLs, multiconductor TLs, and multistory models, which adopt a mixed distributed- and lumped-parameters tower model. Also, results were obtained by FEM or MoM, including the representation of frequency dependent electrical parameters of soil [8–11].

Elementary analyses include the effect of grounding grids through an equivalent lumped resistor whose resistance value is computed at power frequency. More advanced models adopt single or higher-order circuits with lumped parameters, depending on the dimensions of the

* Corresponding author.
E-mail address: erika.stracqualursi@uniroma1.it (E. Stracqualursi).

https://doi.org/10.1016/j.epsr.2024.110866
Received 26 January 2024; Received in revised form 6 June 2024; Accepted 2 July 2024
Available online 18 July 2024

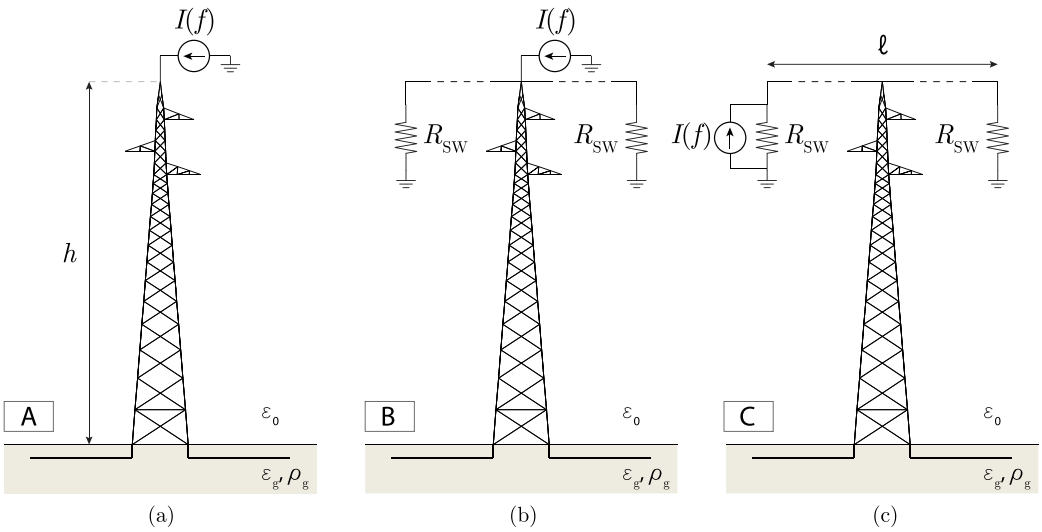

Fig. 1. Schematic representation of the configurations adopted for simulations. (a) Tower and grounding system, with current source connected at the tower top; (b) Tower, grounding system, and shield wire, with current source connected at the tower top; (c) Tower, grounding system, and shield wire, with current source connected at the shield wire termination.

electrodes and soil properties. The frequency trend of the grounding impedance, obtained by simulating only the grounding electrodes in commercial or user-developed full-wave codes, may be included in transient programs as tabulated values or by rational approximating functions derived through the vector fitting technique [12,13].

Comparison of results obtained by these kind of TL models against those found by FEM approaches has not always appeared fully satisfactory [14]. Along with identifying the range of validity of models currently adopted for the different components of power lines (with specific attention to the tower model, which introduces a complex modeling problem [15] since it represents a system of quasi-vertical conductors above the lossy ground), another point to be noted is that only electromagnetic models can account for the effect of EM coupling between different line components (e.g., voltages induced along the grounding electrodes by a current flowing through the shield wire).

The value of the input impedance at the tower top affects the computation of the lightning current division factor [16], hence, the lightning performance of the line too. A good grounding practice favors the reduction of insulation failures between the tower arms and the phase conductors due to lightning overvoltages [17]. This justifies the need for an investigation on the effect of EM coupling between the tower, its grounding system (GS), and shield wire (SW).

The study exploits the computation of input impedances at the node of current injection, to appraise mutual coupling effects primarily in the frequency domain [18]; in the time domain, this is achieved by analyzing the resulting overvoltages obtained by means of numerical Inverse Fourier Transform (IFT).

By means of this analysis, the possibility of excluding any effect of the GS coupling with the tower, and of easily modeling the grounding electrodes by a frequency-dependent grounding impedance is supported, identifying apparent limitations of this approach.

The paper is organized as follows: Section 2 addresses the overview of the simulated configurations, and the rationale underlying their choice; Section 3 recalls the adopted computational approach in the frequency domain; results in both the frequency and the time domain are analyzed in Section 4 to investigate on effects of EM coupling between a reference tower, SW, and GS. Transmission line-type approaches for tower modeling and the use of frequency-dependent approximations of their grounding impedance are considered in Section 5. Conclusive remarks are found in Section 6.

2. Configurations under analysis

In order to assess any effect of the mutual coupling among tower, GS, and SW, the following approach is adopted to carry out the analysis:

1. Only the tower and its GS are considered. The current is injected at the tower top - Case A [Fig. 1(a)].
2. The previous configuration A is modified with the additional simulation of the SW. The latter component is modeled through an horizontal overhead conductor (with diameter $d_0 = 11.5$ mm, and height $h = 31.1$ m), whose length is equal to half a span length, $\ell/2 \cong 200$ m at both sides of the tower top. The current is injected at the tower top - Case B [Fig. 1(b)].
3. The same geometrical configuration of case B is considered; however, the excitation current is injected at the left termination of the simulated overhead conductor - Case C [Fig. 1(c)].

The lightning current is simulated by means of an ideal current source [19]. The choice of not considering the impedance associated with the lightning channel excludes the (frequency-dependent) effects due to an additional current divider at the tower top, and allows to compare the results for the three configurations under the same current excitation. When the SW is included in simulations, it is assumed, as a simplification, that the SW is connected at both terminations to its characteristic resistance defined for the lossless ungrounded case, in order to reduce reflections caused by periodic grounding and by the finite dimensions of the simulated device.

All simulations are performed considering the GS to be buried in a uniform, non-dispersive soil. Following a cartesian approach, the frequency dependence of soil parameters was not considered to prevent the influence on the results of effects different from that on focus in this work. Three different GSs are considered, in order to be able to identify any possible effect associated to longer grounding electrodes on EM coupling. To this aim, the length of the counterpoise wires (with diameter $d_{gs} = 15$ mm) for the three GSs is chosen so that the corresponding grounding resistance at low frequency (100 Hz) is $R_g \cong 20\ \Omega$ [20]. The GSs consist of four counterpoise wires, buried at 0.6 m depth, extending horizontally from the vertices of a square at the soil/air interface with sides equal to 4.8 m (corresponding to the tower base), the shape of the most extended electrodes accounting for the right of way of the line. The main topology of the simulated GSs is represented in Fig. 2; Table 1 includes the values of R_g, the corresponding lengths of the grounding electrodes, and soil resistivity values ρ_g; the constant electric

Table 1
Soil properties and geometrical characteristics for the simulated grounding configurations.

Grounding system	Soil dielectric permittivity ε_g [F/m]	Soil electric resistivity ρ_g [Ω m]	Counterpoise length [m]	Low frequency grounding resistance R_g [Ω]
I: L_1	$80\varepsilon_0$	300	$L_1 = 5.4$	19.79
II: L_1	$80\varepsilon_0$	800	$L_1 = 21.2$	19.76
III: $L_1 + L_2$	$80\varepsilon_0$	2200	$L_1 = 21.2$ $L_2 = 55.0$	19.84

*Sections L_1 and L_2 are indicated in Fig. 2 (not in scale).
**Each buried horizontal electrode is connected to the tower base by a vertical rod (with length 0.6 m).

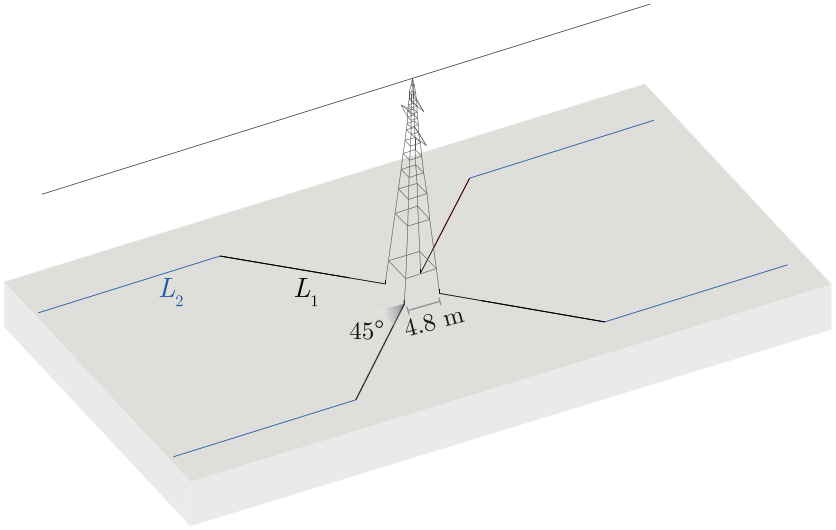

Fig. 2. Configuration under study and topology of the simulated grounding systems; each grounding electrode is subdivided schematically into two main sections, denoted with L_1 and L_2; these sections describe the structure of the simulated grounding systems as from Table 1.

permittivity $\varepsilon_g = 80\varepsilon_0$ was chosen as to approximately consider the order of magnitude of ε_g measured at higher frequencies, where its effects should be most probably observable [21].

The fundamental configurations in Fig. 1 are simulated by means of the hybrid method code [22], briefly recalled in the following section.

3. Hybrid electromagnetic and circuit approach

The device under study is modeled as a conductive structure made of filamentary elements with an assigned radius and finite conductivity. Successively, a mesh generator is used to reduce the structure under study into multiple segments. Nodes are identified with points of connection between two or more segments (or branches). Different approaches for segmentation have been proposed in the literature [23]. In order to unburden the overall computational cost, a different maximum length was chosen for branches located in the air half-space (l_0) or buried in the soil (l_g). These length values were chosen to fulfill the conditions $l_g \ll \lambda_g$ and $l_0 \ll \lambda_0$ at $\hat{f} = 3$ MHz, ensuring the validity of the approximation of electrically short branch at frequencies below $\hat{f}$ (the quantity λ_k, with $k = 0$ and $k = g$, respectively, denotes the computed wavelength in the air and in the soil at $\hat{f}$ [24]).

The block diagram in Fig. 3 schematically represents the workflow of the analysis. Fundamental equations, relevant information, and references, which describe the methodology underlying the computational approach, are addressed in [25,26]. The hybrid method code is given in input data relevant to identify location, length, and interconnections between segments for the structure of interest.

When a known single-tone current is injected at a chosen node, the consequent voltages at the nodes of the structure can be computed while accounting for the EM interactions among segments [22,25]. Considering two branches of the segmented structure, these EM interactions are to be identified with the voltage induced along one segment (due to the magnetic field produced by the current flowing through the other one) and with the leakage current exchanged through their lateral surfaces (associated with the segments' average voltage difference). Hence, it is necessary to compute the produced electric and magnetic fields (or, alternatively, the corresponding potentials), considering their propagation in a multi-layered medium, either the two interacting segments are located in the same layer or in different ones. This is achieved by means of a two-stage procedure:

- computation of the Green's functions for the electric and magnetic potential in the double-layered medium, adopting a spatial–spectral transform [27,28]; the latter transform allows to describe propagation in the vertical direction via an equivalent transmission line approach, using convenient reflection coefficients at the planar interface between the air and the soil half-space;
- computation of the elements of two matrices of frequency-dependent impedances by considering branches in pairs and performing the integration of the Green's functions associated to the source-segment along the victim-segment (representing a self or a mutual impedance term when the source segment does or does not coincide with the victim segment, respectively).

Hence, standard application of the hybrid method code allows to account for EM coupling between all branches.

In the simulation environment, labels are used to mark branches belonging to the mesh of each simulated device. This feature allows to deliberately exclude the effect of mutual EM coupling between different components by assigning a null value to the mutual terms of the aforementioned matrix [25]. While excluding mutual coupling effects, when segments are connected by a common node, wired conduction is always considered as an actual interaction between the simulated components and never excluded.

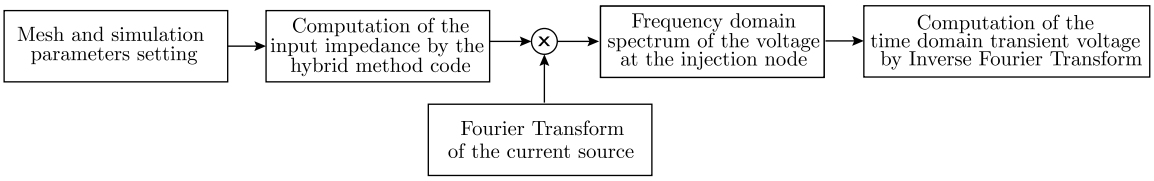

Fig. 3. Workflow diagram, from computation of frequency domain results by the hybrid method code to their particularization in the time domain by Inverse Fourier Transform when a known current source is considered.

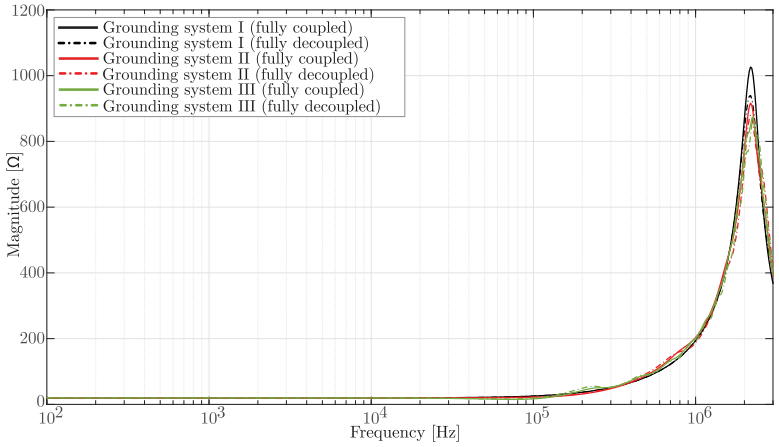

(a) Magnitude of Z_{in}

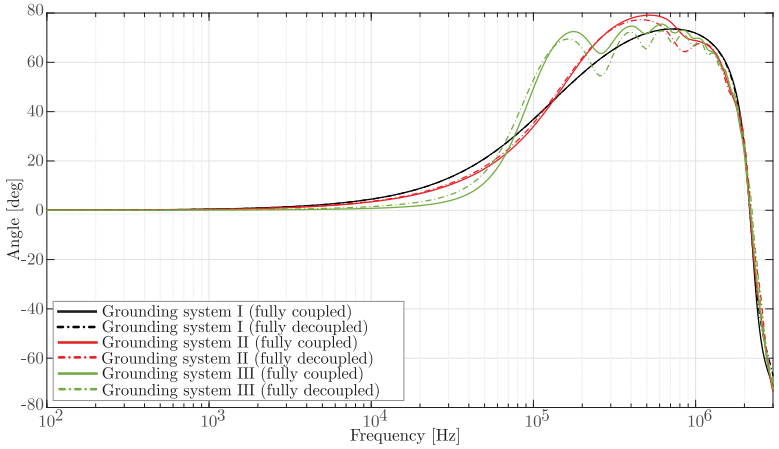

(b) Angle of Z_{in}

Fig. 4. Input impedance, Z_{in}, computed at the tower top by the hybrid method code for the configuration in Fig. 1(a) and grounding systems in Fig. 2 (Table 1); results are computed including or excluding the effect of mutual coupling between tower and grounding system.

When a unit current is injected at a chosen node k, the resulting voltage represents the input impedance, $Z_{\text{in}}(f)$, at this node. However, the differences found in the frequency domain for $Z_{\text{in}}(f)$ in different configurations (e.g., accounting or not for mutual coupling) might be of some interest to transient studies. To this aim, the frequency spectrum, $I(f)$, is computed for a reference current to be injected at node k; the consequent voltage at node k, as a function of time, is calculated by performing the Inverse Fourier Transform of the product $Z_{\text{in}}(f) \cdot I(f)$. In the analysis that follows, a double-peak lightning first stroke is chosen for reference (data required by the corresponding Heidler's functions are found in Table IV of [29], labeled as MSS_FST) [30,31]. This current is selected as a realistic waveform for lightning first strokes, yet statistically representative of the median values of the waveform characteristics.

4. Mutual coupling

In order to take into consideration all the possible EM interactions between tower, GS, and SW, results are first presented for configuration A in Fig. 1(a), which does not account for the SW.

The magnitude and angle of the input impedance, Z_{in}, at the tower top are represented in Fig. 4 for the three GSs. Two plots are associated to each GS: the first one is obtained by considering the segments as fully coupled; the second one removes effects of mutual EM coupling between segments belonging to the tower and to the GS. There seems to be no apparent correlation between the electrodes length and deviations of Z_{in} when excluding coupling effects.

The frequency responses are characterized by some expected features: $Z_{\text{in}} \cong R_{\text{g}}$ at low frequency regardless of the grounding systems,

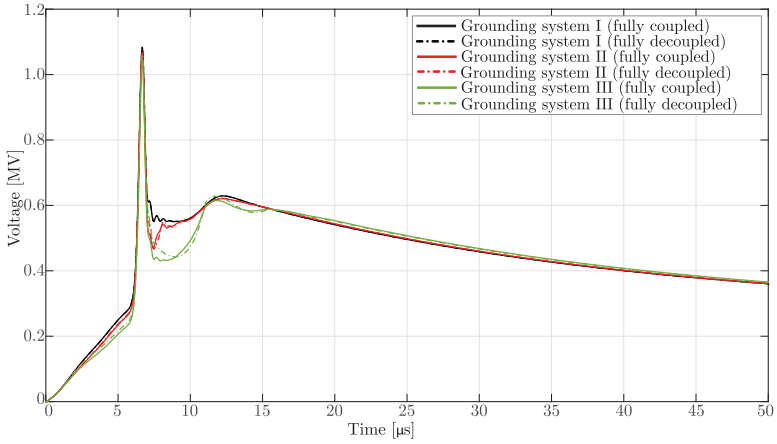

Fig. 5. Voltage computed at the tower top (configuration in Fig. 1(a)) considering or excluding EM coupling effects between the tower and the grounding system, for grounding systems I, II, and III in Table 1 and Fig. 2.

including or not EM coupling; the frequency responses deviate from the low-frequency resistive behavior at a characteristic frequency, F_C, which is smaller for the GS with longer electrodes [24]. The latter effect and the reduced smoothness of frequency responses for the most extended GS corroborate that propagation effects cannot be neglected for electrodes whose lengths are comparable to the minimum wavelength (e.g., with soil properties associated to grounding system III in Table 1, the field wavelength is $\lambda_g \cong 33.5$ m at 1 MHz, which is of the same order of $L_1 + L_2 = 76.2$ m [24]).

Effects associated to the EM coupling between the tower and the GS, although minor, may be observed in the range 500 kHz-1 MHz. More evident effects are observed as the frequency increases: in the range 1–3 MHz, EM coupling effects contribute to increasing the magnitude of Z_{in}, probably due to the predominance of mutual inductive effects in the high-frequency range, as confirmed by the more pronounced inductive behavior of Z_{in} in Fig. 4(b) when fully accounting for tower-GS coupling. This conclusion holds for the three GSs. The largest deviations found for the magnitude are below 10%. However, when performing the IFT to obtain the voltage at node k in the time domain, displayed in Fig. 5, any difference is further weakened by the lightning current frequency spectrum being predominant at $f < 1$ MHz; hence, coupling effects are not practically significant.

Successively, the SW is added to the 3D model, as described in Section 2. Simulations are performed for multiple EM coupling scenarios:

1. fully coupled branches;
2. excluding mutual coupling effects involving the GS;
3. excluding only coupling effects between SW and GS, yet including those ones between tower and SW, and tower with GS;
4. excluding only coupling effects between SW and tower, yet including those ones between tower and GS, and SW and GS;
5. excluding all possible coupling effects between segments belonging to different devices (i.e., SW, tower, and GS are fully decoupled electromagnetically).

Similar results are obtained for the three GSs when modeling the SW and injecting the lightning current at the tower top (as in Fig. 1(b)); hence, results are discussed for grounding systems I and III (i.e., the least and the most extended one, respectively) without limiting the generality of the following observations. From a qualitative analysis of the results, differences among the values of impedance magnitude, computed according to the simulation conditions at points 1–5, may be observed only in the range 1–3 MHz.

Results associated to simulation conditions 1 and 2, allow to focus on the coupling between GS and tower only, confirming that, even in the presence of the SW, the former interaction contributes in increasing the magnitude of Z_{in} in the frequency range close to 1 MHz, as for the case without SW in Fig. 4. It can be noted that the EM coupling between SW and GS has negligible influence on the final value of Z_{in}, being the results superimposed to the ones related to case 1.

However, it is found that the magnitude of Z_{in} at frequencies 1–3 MHz is reduced by excluding all possible mutual coupling between devices (case 5), with both GSs I and III (in Fig. 6 and 7, respectively). The EM interaction between the SW and the tower is identified as the most significant. Indeed, results for case 4, excluding the tower-to-SW EM coupling, show the same patterns as those for case 5. Observing the angle of Z_{in} in Fig. 6(b)-7(b), it can be deduced that considering the latter EM interaction increases the inductive behavior of Z_{in} (especially above 500 kHz). This is confirmed regardless the simulated grounding configuration. Some coupling effects involving the GS may be observed only in Fig. 7, with the longest grounding electrodes (GS III), below 500 kHz.

Given the similarity of results linked to different GSs, voltages in the time domain are displayed only for GS III.

The different coupling scenarios do not lead to any relevant difference in the computed voltages from an engineering point of view, these observations holding for the three GSs under consideration. Furthermore, in Fig. 8 it can be noticed that voltages corresponding to case 1 and 5 are in good agreement, in contrast with the large deviations observed in the frequency domain at 1–3 MHz between Z_{in} for these two cases. This is probably related to the frequency spectrum of the source, enhancing similarities between the corresponding frequency responses in the range 100 kHz-1 MHz.

When the reference current is injected at the SW termination (as in Fig. 1(c)), voltages displayed in Fig. 8 differ from those computed at the tower top both in shape and order of magnitude. This is due to the larger impedance computed in the frequency range 10–100 kHz, of the inductive type, seen at the SW termination (in Fig. 9). However, differences found in the peak values of voltages corresponding to coupling conditions 1–5 are still below 3%.

This last arrangement is proposed as a simplified configuration for simulating midspan current injection in actual transmission lines, and propagation of current along the SW before reaching the tower top. Since mutual coupling effects are negligible for current injection at the tower top, some interest may rise in appraising if any effect due to coupling between the counterpoise electrodes and the SW may be enhanced for current injection along the span, due to their relative position, e.g., the parallel arrangement for case III GS. The magnitude and angle of Z_{in}, linked to the corresponding time domain results in Fig. 8, are displayed in Fig. 9 for GS III (similar results are obtained for the remaining GSs). The different magnitude and shape of the frequency response are related to the chosen point for current excitation.

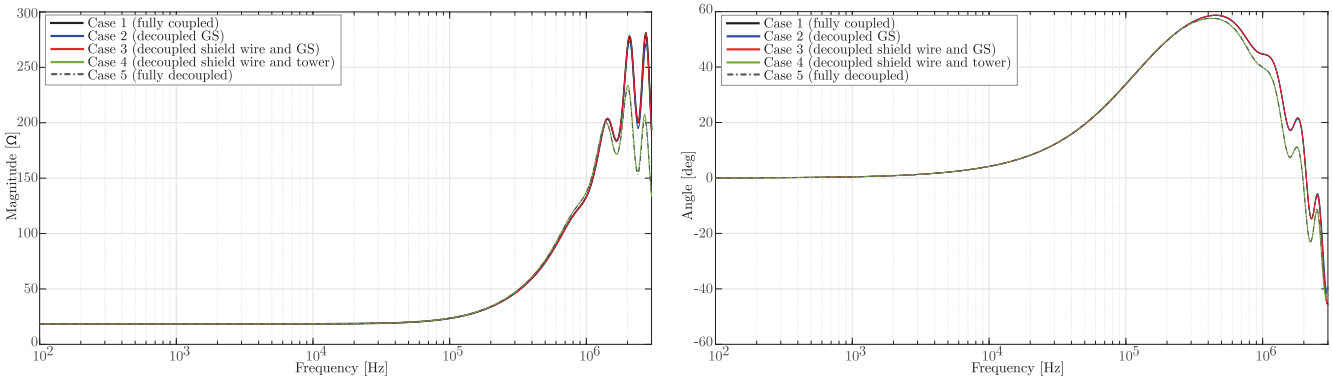

(a) Magnitude of Z_{in} (b) Angle of Z_{in}

Fig. 6. Input impedance at the tower top, Z_{in}, computed by the hybrid method code for the configuration in Fig. 1(b) and grounding system I in Table 1 and Fig. 2, with different coupling scenarios between tower, grounding system and shield wire.

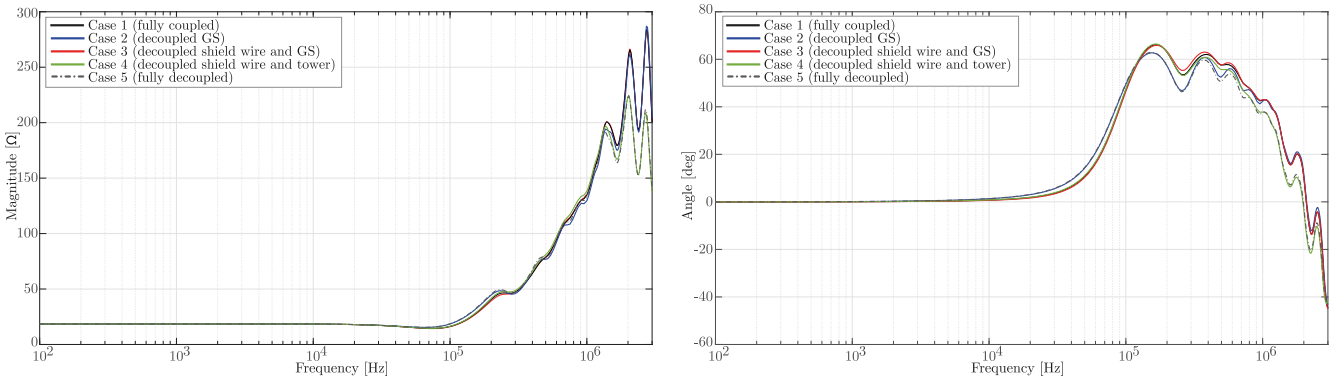

(a) Magnitude of Z_{in} (b) Angle of Z_{in}

Fig. 7. Input impedance at the tower top, Z_{in}, computed by the hybrid method code for the configuration in Fig. 1(b) and grounding system III in Table 1 and Fig. 2, with different coupling scenarios between tower, grounding system and shield wire.

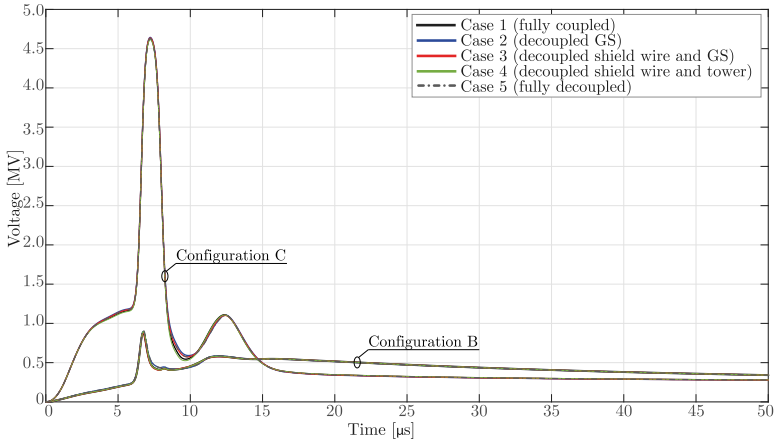

Fig. 8. Voltages at the tower top (Fig. 1(b)) and at the shield wire termination (Fig. 1(c)) computed according to different coupling scenarios, with grounding system III in Table 1 and Fig. 2.

In fact, the characteristic frequency at which the input impedance, Z_{in}, deviates from its low-frequency value ($|Z_{\text{in}}| \cong 18.9\,\Omega$) is lower when it is computed at the SW termination; this is due to the equivalent length of the overall structure seen at the point of current excitation, which includes the tower, the GS, and the whole simulated span (differently from the previous cases, in which two parallel half-spans were seen at the tower top for the computation of Z_{in}). Similar observations hold as to the influence of EM coupling between components, confirming the tower-to-SW interaction as the most relevant, mainly in the range 1–3 MHz.

4.1. Impulse impedance of grounding systems

Two additional grounding systems were simulated to extend the degree of generality of our conclusions, displaying different values of impulse grounding impedance, z_i, compared to those of GSs I-III

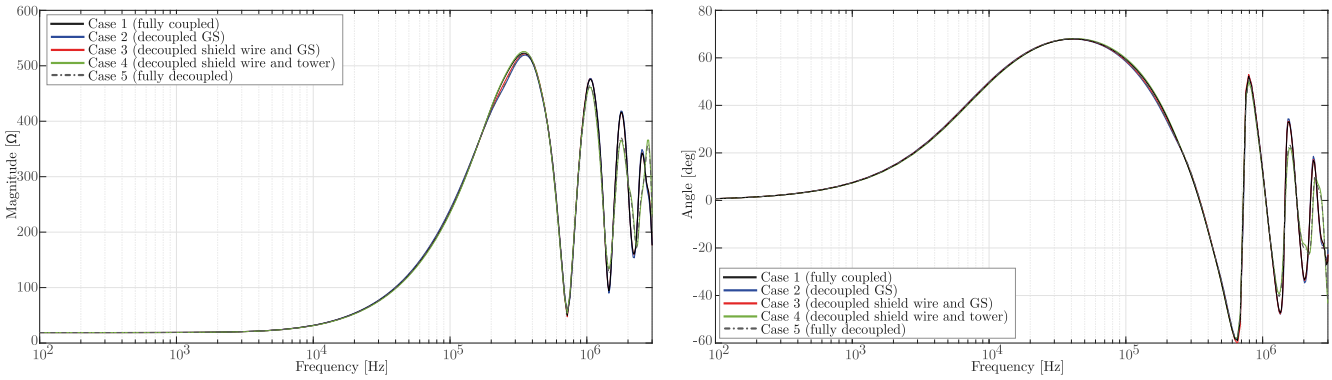

(a) Magnitude of Z_{in} (b) Angle of Z_{in}

Fig. 9. Input impedance at the shield wire termination, Z_{in}, computed by the hybrid method code for the configuration in Fig. 1(c) and grounding system III in Table 1 and Fig. 2, with different coupling scenarios between tower, grounding system and shield wire.

Table 2
Soil properties and geometrical characteristics for the additional grounding configurations.

Grounding system	Soil dielectric permittivity ε_g [F/m]	Soil electric resistivity ρ_g [Ω m]	Counterpoise length [m]	Low frequency grounding resistance R_g [Ω]
IV: L_1	$80\varepsilon_0$	800	L_1 = 10.8	32.75
V: L_1+L_2	$80\varepsilon_0$	800	L_1 = 30.0 L_2 = 25.0	9.30

*Sections L_1 and L_2 are indicated in Fig. 2 (not in scale).
**Each buried horizontal electrode is connected to the tower base by a vertical rod (with length 0.6 m).

Table 3
Impulse impedance for the considered grounding systems.

Grounding system	I	II	III	IV	V
Grounding resistance, R_g [Ω]	19.79	19.76	19.84	32.75	9.30
Impulse grounding impedance, z_i [Ω]	19.76	19.67	19.36	32.62	9.43

(details are listed in Tables 2 and 3) [32]. The input impedances computed considering these GSs are not displayed, since the results are aligned to those previously discussed; this observation applies also to the configurations with GS IV, which is expected to enhance any effect linked to the portion of lightning current flowing vertically to the soil (due to the lower z_i).

It should be noted that only GS V displays an impulse impedance $z_i > R_g$. This is because each counterpoise electrode is longer than the effective length associated with the considered soil properties (ρ_g = 800 Ωm) and typical first return stroke currents [32].

5. Assessment of macromodeling approaches

In Fig. 5, considering configuration A and the chosen lightning current, it was shown that the differences found in the frequency-domain results among the different simulated coupling scenarios are partially identifiable in the time-domain results. It is confirmed also by results in Fig. 8 for configuration B and C, including the shield wire. This observation supports the applicability of a macromodeling approach, provided that convenient equivalent circuit models are chosen for each device. In power system transient studies, aerial conductors are usually simulated by the well-established transmission line model, neglecting the propagation of any mode of order higher than the TEM mode [33]. Hence, configuration A is investigated in this section, since it highlights the effects of different modeling choices for the simulation of the tower and the grounding system.

Based on the tower models reviewed thoroughly in [5], considering the arrangement A in Fig. 1, and adopting $0.9\,c_0$ as propagation velocity along the tower, multistory tower models qualitatively result in a closer approximation of the input impedance at the tower top computed by the hybrid approach in Section 4; when it comes to towers whose grounding electrodes are buried in a soil with finite conductivity, this can be observed in Fig. 10, representing the input impedance at the tower top, as obtained by Jordan's and Motoyama et al. models for the tower under analysis with GS III (the parameters used for the tower models are in Table 4 [5]).

Similarly to Jordan's model results in Fig. 10, lossless models introduce sharp resonances at high frequencies which do not have a counterpart in the output obtained by the hybrid method code; multistory models, instead, may represent a good starting point to obtain more accurate approximations of Z_{in} for suitable values of the characteristic impedances and damping elements within each story.

Hence, Motoyama et al. formula was selected, as a representative of multistory models, to assess results in the time domain; the same first stroke current was used to compute the overvoltage at the tower top for configuration A in Fig. 1. Having shown that the coupling between tower and GS holds negligible influence on the computation of overvoltages at the tower top, only the most extended GS is considered here, being its dimensions such to make propagation effects along the counterpoise wires more relevant (thus, being less suitable for lumped parameters representation of its grounding impedance). Considerations are made with respect to results computed by the hybrid method code excluding mutual coupling effects between the tower and the GS.

The GS frequency response was simulated through different approaches, commonly adopted in the context of macromodeling procedures: by a single R-L circuit, by the series of an R-L circuit with an R-C parallel, and by using the GS response, as computed by the hybrid method. The first two frequency-dependent models were obtained by application of vector fitting [12], by forcing 1 and 2 poles for the rational function approximating the grounding admittance computed by the hybrid method code. These latter approximations with few poles were considered in order to provide an insight on the effect of adopting very simple lumped-parameters models for extended GSs, which cannot reproduce accurately the frequency dependence of the corresponding grounding impedance.

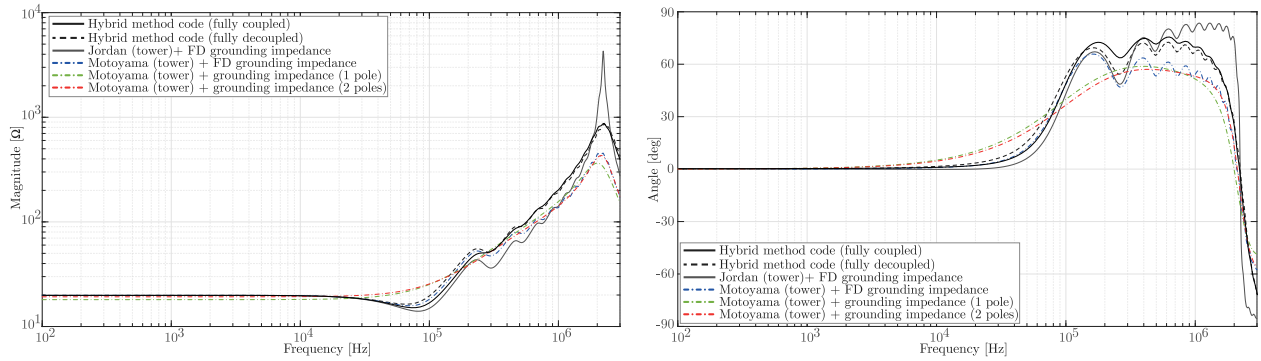

(a) Magnitude of Z_{in} (b) Angle of Z_{in}

Fig. 10. Input impedance at the tower top, Z_{in}, for configuration A in Fig. 1 and grounding system III in Table 1 and Fig. 2. Z_{in} is computed by the hybrid method code or by Motoyama et al. tower model with different approximations for the grounding system admittance (a frequency-dependent (FD) function obtained by the hybrid method code, or approximated by 1 or 2 poles rational functions). Results by Jordan's model are included for comparison.

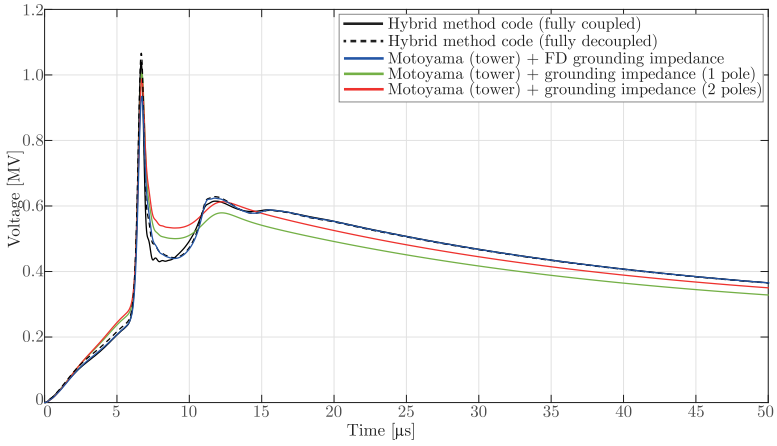

Fig. 11. Voltages at the tower top for configuration A in Fig. 1 and grounding system III, computed by the hybrid method code and by applying Motoyama et al. tower model with different approximations for the grounding admittance (a frequency-dependent (FD) function obtained by the hybrid method code, or approximated by 1 or 2 poles rational functions).

In Fig. 11, lumped-parameters modeling for the GS impedance leads to different voltage waveforms compared to results employing the hybrid code output for Z_{in} (used as reference); this can be observed not only at the voltage front and peak in Fig. 11, but also at later times, e.g., after 7 μs, due to the alteration of the reflection coefficient at the tower footing and to the less accurate approximation of the low-frequency resistive behavior of the grounding impedance. The voltage waveform computed combining the chosen multistory tower model with the exact frequency response of the GS is in satisfactory agreement throughout the displayed time interval, although a larger discrepancy, around 12%, is found for the peak value; with the hybrid method-computed GS response, this deviation should be only ascribed to the goodness of the chosen tower model and its parameters. Voltage peak values calculated with the simpler lumped-parameters circuits are closer to the reference case: this observation is bound to the specific raw approximations used for the equivalent circuit of GS III, which partially disguise the effect of the chosen tower equivalent model on the computed Z_{in}.

The GS admittance approximation by a two-poles rational function represents an improvement with respect to a simple R-L circuit, as to the overall approximation of the voltage waveform.

The accurate simulation of the GS admittance, e.g., by means of rational functions with a sufficient number of poles, is fundamental to accurately predict the voltage front and waveshape, relevant for insulation flashover studies.

This is further confirmed in Fig. 12, accounting for different multistory tower models (with parameters in Table 4, and $R_5 = 0$ for Baba et al. model [5]) in combination with the non-approximated frequency-dependent response of the GS; the latter representation of the frequency-dependent behavior of the GS is essential for accurate results, when plotting voltages obtained by application of those macromodeling approaches against the voltage obtained with Z_{in} computed solely by the hybrid method code.

In this case, the most evident deviations are found at the first peak. In order to attenuate those latter differences, approximately in the range ±12% for the configuration under study, room for improvement is left only as to the chosen tower model and parameters. In this respect, one should expect the damping of voltage waves propagating along the tower to be also related to the properties of the underlying soil, influencing the solution of the EM problem; however, common multistory models are based on empirical evidence, and do not put in relation the tower model's parameters and damping circuit elements to the local soil properties.

6. Conclusion

This paper is an additional contribution to an ongoing study on electromagnetic mechanisms involving towers of overhead transmission lines. The results of simulations show that neglecting electromagnetic coupling effects between the tower and the shield wire affects the input impedance (calculated at the current excitation node) only in

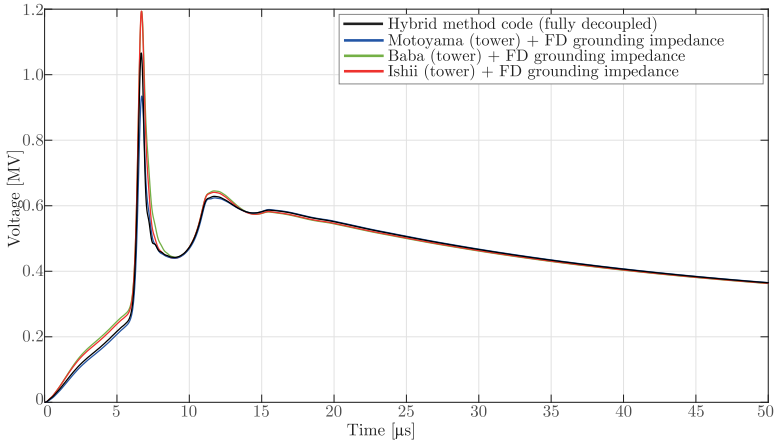

Fig. 12. Voltages at the tower top for configuration A in Fig. 1 computed by the hybrid method code and by different multistory models (i.e., tower models by Motoyama et al., Baba et al., and Ishii et al.) when considering the frequency-dependent (FD) impedance of GS III (as computed by the hybrid method code).

Table 4
Parameters adopted for the considered tower models [5].

Tower model	Parameters description	Ref.
Corrected Jordan	$Z = 177\,\Omega$	[34,35]
Motoyama et al.	$Z_i = 120\,\Omega$, $i = 1, \dots, 4$, $\gamma = 0.8$	[36]
Baba et al.	$Z_1 = Z_2 = 200\,\Omega$, $Z_3 = 180\,\Omega$, $Z_4 = 150\,\Omega$, $R_2 = 20\,\Omega$, $R_3 = 30\,\Omega$, $R_4 = 25\,\Omega$, $L_2 = 4.6\,\mu H$, $L_3 = 6.9\,\mu H$, $L_4 = 11.5\,\mu H$	[37]
Ishii et al.	$Z_1 = Z_2 = Z_3 = 220\,\Omega$, $Z_4 = 150\,\Omega$, $R_1 = 20\,\Omega$, $R_2 = 17\,\Omega$, $R_3 = 12\,\Omega$, $R_4 = 33\,\Omega$, $L_1 = 4.6\,\mu H$, $L_2 = 3.8\,\mu H$, $L_3 = 2.8\,\mu H$, $L_4 = 7.7\,\mu H$	[38]

*Parameters refer to the tower equivalent circuits reviewed in [5].

the higher frequency range (above 1 MHz); this corresponds to minor differences in the simulated tower top voltages when considering a current waveform with median values of its characteristic parameters. Lightning currents with slower (faster) fronts are expected to reduce (enhance) the effects of tower-to-shield wire coupling.

Coupling effects between the tower and the grounding electrodes practically do not affect the input impedance. Therefore, considering the frequency spectra of lightning currents, coupling influence is very slight in terms of resulting overvoltages. The possibility of not considering the coupling effects linked to grounding electrodes has been proved a reasonable engineering approach for studies of lightning performance of transmission lines, denoted in the work by considering arrangements of grounding electrodes corresponding to specific values of impulse impedance. Hence, the results of this work confirm the suitability of simulating the grounding system by a frequency-dependent parameter in the study of complex power systems, and adopting the macro-modeling approach typical of electromagnetic transients programs. In addition to the concern related to accuracy, this approach allows minimizing the computational workload when simulating analogous configurations through the utilization of codes and software with core theory akin to the one implemented by the hybrid method code.

CRediT authorship contribution statement

Erika Stracqualursi: Writing – original draft, Software, Methodology, Investigation, Formal analysis, Conceptualization. **Rodolfo Araneo:** Writing – original draft, Supervision, Software, Formal analysis, Conceptualization. **Amedeo Andreotti:** Writing – original draft, Supervision, Formal analysis, Conceptualization. **José Brandão Faria:** Writing – original draft, Supervision, Formal analysis. **Fernando H. Silveira:** Writing – original draft, Supervision, Investigation, Formal analysis, Conceptualization. **Silverio Visacro:** Writing – original draft, Supervision, Investigation, Formal analysis, Conceptualization.

Declaration of competing interest

The authors declare that they have no known competing financial interests or personal relationships that could have appeared to influence the work reported in this paper.

Data availability

Data will be made available on request.

Acknowledgments

The work of E. Stracqualursi was funded under the National Recovery and Resilience Plan (NRRP), Mission 4 Component 2 Investment 1.3 - Call for tender No. 1561 of 11.10.2022 of Ministero dell'Università e della Ricerca (MUR); funded by the European Union – NextGenerationEU (Project code PE0000021, Concession Decree No. 1561 of 11.10.2022 adopted by Ministero dell'Università e della Ricerca (MUR), CUP B53C22004070006, Project title "Network 4 Energy Sustainable Transition – NEST").

References

[1] S. Grivet-Talocia, B. Gustavsen, Passive macromodeling: Theory and applications, John Wiley & Sons, 2015.
[2] C.R. Paul, Analysis of Multiconductor Transmission Lines, John Wiley and Sons, 2008.
[3] S. Visacro, A. Soares, HEM: A model for simulation of lightning-related engineering problems, 20 (2) (2005) 1206–1208.
[4] J.A.M. Velasco, Power system transients: Parameter determination, CRC Press, 2010.
[5] E. Stracqualursi, G. Pelliccione, S. Celozzi, R. Araneo, Tower models for power systems transients: A review, Energies 15 (13) (2022) 4893.
[6] F.S. Almeida, F.H. Silveira, A. De Conti, S. Visacro, Influence of tower modeling on the assessment of backflashover occurrence on transmission lines due to first negative lightning strokes, Electr. Power Syst. Res. 197 (2021) 107307.
[7] Z.G. Datsios, P.N. Mikropoulos, Effect of tower modelling on the minimum backflashover current of overhead transmission lines, in: 19th International Symposium on High Voltage Engineering (ISH), Pilsen, Czech Republic, 2015.
[8] D. Cavka, N. Mora, F. Rachidi, A comparison of frequency-dependent soil models: Application to the analysis of grounding systems, IEEE Trans. Electromagn. Compat. 56 (1) (2014) 177–187.
[9] A.R.J. de Araújo, J.S.L. Colqui, C.M. de Seixas, S. Kurokawa, B. Salarieh, J. Pissolato Filho, B. Kordi, Computation of ground potential rise and grounding impedance of simple arrangement of electrodes buried in frequency-dependent stratified soil, Electr. Power Syst. Res. 198 (2021) 107364.
[10] S. Visacro, R. Alipio, Frequency dependence of soil parameters: Experimental results, predicting formula and influence on the lightning response of grounding electrodes, IEEE Trans. Power Del. 27 (2) (2012) 927–935.
[11] R. Alipio, S. Visacro, Frequency dependence of soil parameters: Effect on the lightning response of grounding electrodes, IEEE Trans. Electromagn. Compat. 55 (1) (2013) 132–139.

[12] B. Gustavsen, A. Semlyen, Rational approximation of frequency domain responses by vector fitting, IEEE Trans. Power Del. 14 (3) (1999) 1052–1061.
[13] B. Gustavsen, Improving the pole relocating properties of vector fitting, IEEE Trans. Power Del. 21 (3) (2006) 1587–1592.
[14] M. Ghomi, H. Zhang, C.L. Bak, F.F. da Silva, K. Yin, Integrated model of transmission tower surge impedance and multilayer grounding system based on full-wave approach, Electr. Power Syst. Res. 198 (2021) 107355.
[15] E. Stracqualursi, R. Araneo, J. Brandão Faria, P. Burghignoli, A. Andreotti, B. Kordi, On the transient analysis of towers: A revised theory based on sommerfeld-goubau wave, IEEE Trans. Power Deliv. 38 (1) (2022) 309–318.
[16] R. Zeng, J. He, B. Zhang, Methodology and technology for power system grounding, John Wiley & Sons, 2012.
[17] S. Visacro, F.H. Silveira, Review of measures to improve the lightning performance of transmission lines, Electr. Power Syst. Res. 213 (2022) 108729.
[18] E. Stracqualursi, R. Araneo, A. Andreotti, J. Brandão Faria, F.H. Silveira, S. Visacro, Computation of the input impedance of transmission towers: Effects of macromodeling, in: Proceedings of International Conference on Grounding & Lightning Physics and Effects (GROUND 2023 & 10th LPE), 2023, pp. 1–4.
[19] Working Group C4.407, V. Rakov, A. Borghetti, C. Bouqeugneau, W. Chisholm, K. Cummins, G. Diendorfer, F. Heidler, A. Hussein, M. Ishii, C. Nucci, A. Piantini, O. Pinto, X. Qie, F. Rachidi, M. Saba, T. Shindo, W. Schulz, R. Thottappillil, S. Visacro, W. Zischank, Lightning parameters for engineering applications, Brochure 549 (2013).
[20] Z.G. Datsios, E. Stracqualursi, R. Araneo, P.N. Mikropoulos, T.E. Tsovilis, Estimation of the minimum backflashover current and backflashover rate of a 150 kV overhead transmission line: Frequency and current-dependent effects of grounding systems, in: 2022 22nd IEEE Int. Conf. Environ. and Electr. Eng., 2018-06, pp. 1–5.
[21] R. Alipio, S. Visacro, Modeling the frequency dependence of electrical parameters of soil, IEEE Trans. Electromagn. Compat. 56 (5) (2014) 1163–1171.
[22] E. Stracqualursi, R. Araneo, Transient impedance of grounding grids with different soil models, in: 2021 IEEE Int. Conf. Environ. and Electr. Eng., 2021, pp. 1–6.
[23] M.A.O. Schroeder, R.A.R. de Moura, V.M. Machado, A discussion on practical limits for segmentation procedures of tower-footing grounding modeling for lightning responses, IEEE Trans. Electromagn. Compat. 62 (6) (2020) 2520–2527.
[24] L. Grcev, High-frequency grounding, in: Lightning Protection, IET, 2010, pp. 503–529.
[25] E. Stracqualursi, Analysis of actual multiconductor transmission lines: effects of non-uniformities and nonlinearities (Ph.D. thesis), Sapienza University of Rome, 2023.
[26] E. Stracqualursi, R. Araneo, GEA simulator: Power frequency and transient simulations for practical applications, in: 2024 IEEE Int. Conf. Environ. and Electr. Eng., 2024, pp. 1–6, in press.
[27] V.N. Kourkoulos, A.C. Cangellaris, Accurate approximation of Green's functions in planar stratified media in terms of a finite sum of spherical and cylindrical waves, IEEE Trans. Antennas Propag. 54 (5) (2006) 1568–1576.
[28] K.A. Michalski, J.R. Mosig, Multilayered media Green's functions in integral equation formulations, IEEE Trans. Antennas Propag 45 (3) (1997) 508–519.
[29] F.H. Silveira, A. De Conti, S. Visacro, Lightning overvoltage due to first strokes considering a realistic current representation, IEEE Trans. Electromagn. Compat. 52 (4) (2010) 929–935.
[30] A. De Conti, S. Visacro, Analytical representation of single- and double-peaked lightning current waveforms, IEEE Trans. Electromagn. Compat. 49 (2) (2007) 448–451.
[31] S. Visacro, A representative curve for lightning current waveshape of first negative stroke, Geophys. Res. Lett. 31 (7) (2004).
[32] S. Visacro, The use of the impulse impedance as a concise representation of grounding electrodes in lightning protection applications, IEEE Trans. Electromagn. Compat. 60 (5) (2018) 1602–1605.
[33] R. Lings, EPRI AC Transmission line reference book: 200 kV and above, third ed., Electric Power Research Institute, Palo Alto, 2005.
[34] A. De Conti, S. Visacro, A. Soares, M.A.O. Schroeder, Revision, extension, and validation of Jordan's formula to calculate the surge impedance of vertical conductors, IEEE Trans. Electromagn. Compat. 48 (3) (2006) 530–536.
[35] H. Takahashi, Confirmation of the error of Jordan's formula on tower surge impedance, IEEJ Trans. Power Energy 114 (1) (1994) 112–113.
[36] H. Motoyama, K. Shinjo, Y. Matsumoto, N. Itamoto, Observation and analysis of multiphase back flashover on the okushishiku test transmission line caused by winter lightning, IEEE Trans. Power Del. 13 (4) (1998) 1391–1398.
[37] Y. Baba, M. Ishii, Tower models for fast-front lightning currents, IEEJ Trans. Power Energy 120 (1) (2000) 18–23.
[38] M. Ishii, T. Kawamura, T. Kouno, E. Ohsaki, K. Shiokawa, K. Murotani, T. Higuchi, Multistory transmission tower model for lightning surge analysis, IEEE Trans. Power Del. 6 (1991) 1327–1335.